Research Square

Preprints are preliminary reports that have not undergone peer review.
They should not be considered conclusive, used to inform clinical practice,
or referenced by the media as validated information.

Analysis of the Vibration Characteristics and Transmission Paths of Rail Trains Based on OTPA

Yuqi Cheng
East China Jiaotong University
Qian Xiao
7453575880qq.com

East China Jiaotong University
Chao Chang
East China Jiaotong University
Hesheng Liu
East China Jiaotong University
Huanhuan Li
Jiangxi Vocational College of Mechanical & Electrical Technology
Hu Zeng
Jiangxi Vocational College of Mechanical & Electrical Technology

---

Article

Keywords: Rail train, Vibration characteristics, Operational Transfer Path Analysis, Frequency modulation, Transfer function

Posted Date: August 19th, 2026

DOI: https://doi.org/10.21203/rs.3.rs-10542314/v1

License: This work is licensed under a Creative Commons Attribution 4.0 International License.
Read Full License

Additional Declarations: No competing interests reported.

Analysis of the Vibration Characteristics and Transmission Paths of Rail Trains Based on OTPA

Yuqi Cheng[1,2], Qian Xiao[1]*, Chao Chang[1],Hesheng Liu[1], Huanhuan Li[2], Hu Zeng[2]

(1.Railway Industry Key Laboratory of Intelligent Operation and Maintenance of Rolling stockt, East China Jiaotong University, Nanchang 330013, Jiangxi, China;

2.Jiangxi Vocational College of Mechanical & Electrical Technology, Nanchang 330013, Jiangxi, China)

Abstract: The operational conditions of urban rail transit trains are intricate. With the increasing speed of rail trains, external excitations grow continuously, causing significant vibrations in the train. These lead to a decline in passenger riding comfort. In severe cases, they may even cause lateral instability of the train, endangering traffic safety.Therefore, it is of great significance to study the vibration characteristics of key train components and the specific paths through which vibrations are transmitted from outside to inside the vehicle.In this paper, the authors affixed a number of vibration acceleration sensors to the key components of a metro train and carried out tracking tests.Vibration characteristics of the train under different working conditions were obtained, and the characteristic frequencies of key components such as axle boxes, motors, gearboxes, bogie frames, and car bodies were analyzed.The OTPA (Operational Transfer Path Analysis) method was employed to establish two-level vertical transfer paths: "outer car body to interior floor" and "bogie frame to center pin of outer car body".Then, the vertical transfer function of vibrations from axle boxes to bogie frames was analyzed. By evaluating the contribution of each excitation source to response points, the main transfer paths of interior car body vibrations were determined.The results show that obvious frequency-modulation phenomena occur in the vibration characteristics of axle boxes, gearboxes and motors. The related characteristic frequencies are related to the wheel polygon orders, sleeper spacing, motor orders, and the meshing frequencies of large and small gears.Vibrations are transmitted from the axle boxes through the bogie frame to the car body, with a vibration attenuation rate of approximately 0.1. Excitations caused by wheel polygonization and track irregularities are mainly transmitted through primary steel springs and primary vertical dampers, passing through the mid-section of bogie side beams and bogie crossbeams, and finally transferred to the car interior via anti-hunting dampers and center pins.The research work in this paper provides an effective reference for the structural optimization and vibration-noise reduction of rail trains.

Keywords: Rail train; Vibration characteristics; Operational Transfer Path Analysis; Frequency modulation; Transfer function

1. Introduction

Rail transit trains have become a vital mode of transportation for commuting and daily travel. With the continuous increase in operating speeds and passenger capacities, ride comfort has garnered growing attention. However, rail vehicles are subjected to various impact loads due to external factors

*Corresponding author

*E-mail addresses:*17770844981@163.com (Y. Cheng), 745357588@qq.com(Q. Xiao), changchao2018@my.swjtu.edu.cn(C.Chang), hsliu@vip.163.com (H. Liu), huanz1224@163.com(H. Li), 371749840@qq.com (H. Zeng)

such as wheel-rail wear and operational environmental conditions[1]. These loads can induce abnormal vibrations in both the bogie and the vehicle interior[2-4], potentially triggering vehicle fault alarms or even unscheduled stops in severe cases, thereby significantly compromising safety, operational stability, and passenger comfort[5-7]. Consequently, investigating the vibration characteristics of trains and their transmission mechanisms is of critical importance for structural optimization, health monitoring, and vibration/noise mitigation strategies.

Numerous scholars have investigated the vibration characteristics of vehicle systems. Ai et al. [8] and Hu et al. [9] constructed dynamic simulation models to analyze the vibration frequencies of gearbox housings under wheel-rail excitations. Guo [10] studied the vibration behavior of high-speed train carbody and its suspended components, examining wheel-rail interactions and vehicle running stability, while also analyzing the time-frequency and frequency-domain characteristics of carbody vibrations. Sun [11] conducted comprehensive experiments on actual traction motors of high-speed trains, and leveraging the inherent property of induction motors—where cage faults can be reflected in the stator current via air-gap magnetic field modulation—proposed a method for monitoring the health status of traction motor bearing cages based on stator current analysis, thereby enabling vibration monitoring and investigation of bearing dynamics. Lin Fengtao [12] established a high-speed train dynamic simulation model to investigate the influence of different wheel polygonalization amplitudes on the train's vibration characteristics. However, most of these studies are based on simulation models and primarily focus on the vibration analysis of key components, with limited attention paid to the overall vehicle's vibration transmission and attenuation mechanisms.Shi Huailong [13] conducted long-term field tracking tests on a high-speed train, systematically analyzing the statistical patterns of vibration accelerations at the axle box, bogie frame, and carbody under various wheel wear conditions. Xu Ning [14] performed field measurements on the Wuhan–Guangzhou high-speed railway line, acquiring vertical and lateral vibration acceleration time histories of critical components such as the axle box, carbody, bogie frame, gearbox, and brake hanger mounts. The study further analyzed the overall vibration attenuation characteristics of the train and the vibration transmission behavior of key components. These field test studies provide valuable data support for theoretical and numerical investigations and partially reveal the vibration characteristics and attenuation patterns of trains. However, they still fail to clearly identify the specific vibration transmission paths, and thus cannot fully or comprehensively represent the overall vibration transmission mechanisms in railway vehicles.

To elucidate the vibration transmission mechanisms of railway vehicles, transfer path analysis (TPA) is required. TPA is a powerful methodology capable of identifying dominant excitation sources and their associated transmission paths, thereby facilitating the resolution of noise, vibration, and harshness (NVH) issues. Although TPA has been extensively applied in fields such as automotive and marine engineering [15-17], its adoption in railway applications remains relatively limited. In particular, TPA proves highly effective in analyzing vibration transmission in complex vehicle systems and holds significant potential for guiding vibration mitigation strategies and structural optimization [18-20].

Transfer path analysis (TPA) can be broadly classified into three categories: classical TPA, component-based TPA, and Operational Transfer Path Analysis (OTPA) [21]. Classical TPA delivers accurate analytical results by leveraging frequency response functions (FRFs); however, the effective measurement of FRFs is often challenging in real-world engineering scenarios [22-23]. In comparison with classical TPA, component-based TPA simplifies the experimental procedure through the

introduction of blocked forces, yet it still relies on precise FRFs between the active and passive subsystems [24-25]. Although both classical and component-based TPA approaches can yield reliable outcomes, their high implementation costs and substantial resource demands significantly hinder their practical applicability. In contrast, OTPA replaces FRFs with transmissibility functions, offering distinct advantages in terms of ease of implementation and low resource consumption.

Operational Transfer Path Analysis (OTPA) enables quantitative assessment of the contribution from individual excitation sources to target response points within the vehicle interior, thereby facilitating the identification of specific vibration transmission paths [26-28]. In contrast to conventional TPA methods, OTPA requires only the operational excitation signals and the corresponding response signals at target locations to compute path transmissibilities and contribution levels [29-31]. This approach can be implemented without disassembling or isolating the excitation sources, allowing simultaneous measurement of all relevant transmission paths under real operating conditions [32-34]. However, to ensure the reliability of the results, appropriate methodologies must be employed to address issues such as path coupling and signal crosstalk [35].

In this study, a certain type of rail vehicle is taken as the research object. Vibration acceleration signals are collected from key components of the train, including axle boxes, motors, gearboxes, bogie frames, and carbody. The vibration characteristics under different operating conditions—such as acceleration, constant-speed operation, and between leading and trailing cars—are investigated. Statistical properties of the vehicle system's vibration accelerations, vibration attenuation behavior, and characteristic frequencies at measurement points under various operating conditions are analyzed. Subsequently, a two-stage Operational Transfer Path Analysis (OTPA) model is established, where the first-stage OTPA path is defined as "external carbody to interior floor" and the second-stage path as "bogie frame to external carbody." The contribution of each excitation source to the vibration responses at the interior floor and external carbody is calculated. By analyzing various time-and frequency-domain characteristics, this study aims to more completely and accurately reveal the vibration behavior and transmission paths of rail vehicles during service, providing valuable reference for the rational operation and design of rail vehicles, as well as for simulation and theoretical research.

1 Railway Train Tracking Test

Due to the high sensor demand in vibration transfer path analysis experiments, a total of 27 triaxial acceleration sensors were employed in this test. For data acquisition, the HEADlab system was selected, which is a portable, modular, multi-channel data acquisition platform. The post-processing and Operational Transfer Path Analysis (OTPA) synthesis were performed using ArtemiS SUITE software. The specific configuration of the sensors, the HEADlab acquisition front-end, and their in-vehicle layout are illustrated in Figure 1.



Fig.1 triaxial vibration acceleration sensors (left), HEADlab digital acquisition front (center), and in-cabin layout of the acquisition hardware (right)

A leading car of a rail vehicle was selected as the research subject. To account for the influence of wheel–rail excitations and the traction motor on the carbody vibration system, triaxial vibration acceleration sensors were installed at key locations, including the interior floor, the connection points between the secondary suspension components at the first end of the bogie and the carbody, the bogie frame, axle boxes, gearboxes, and motor frames. To ensure measurement accuracy and sufficient coverage of the dominant vibration frequencies in the railway vehicle system, appropriate sampling frequencies and sensor ranges were selected, as detailed in Table 1. Due to the close proximity of their mounting positions, the anti-yaw dampers and the anti-roll torsion bars share a common measurement point on the frame side. Similarly, the air springs and vertical dampers also share a single frame-side measurement location. Figure 2 illustrates the vibration transmission paths and the positions of selected acceleration sensor measurement points.

Table1. Arrangement positions, sampling frequencies and measurement ranges of each measuring point

Measuring point range	Measurement point number	Measuring point position	Channel number			Sampling frequency (Hz)	Measurement range (g)
			X	Y	Z		
Inside the carriage	P1	Front-end floor of the car body	1	2	3	500	5
	P2	Seat	4	5	6	500	5
	P3	Central floor of the car body	7	8	9	500	5
Outside the car body	P4	Left-side anti-yaw damper at carbody end	10	11	12	500	5
	P5	Right-side anti-yaw damper at carbody end	13	14	15	500	5
	P6	Left-side anti-roll torsion bar at carbody end	16	17	18	500	5
	P7	Right-side anti-roll torsion bar at carbody end	19	20	21	500	5
	P8	Left-side air spring/vertical damper at carbody end	22	23	24	500	5
	P9	Right-side air spring/vertical damper at carbody end	25	26	27	500	5

	P10	Center pin	28	29	30	500	5
	P11	Connection between traction inverter and carbody	31	32	33	500	5
No.1 end bogie	P12	Left-side anti-yaw damper and anti-roll torsion bar at bogie frame end	34	35	36	2000	50
	P13	Right-side anti-yaw damper and anti-roll torsion bar at bogie frame end	37	38	39	2000	50
	P14	Left-side air spring and vertical damper at bogie frame end	40	41	42	2000	50
	P15	Right-side air spring/vertical damper at frame end	43	44	45	2000	50
	P16	Left-side secondary transverse damper at frame end	46	47	48	2000	50
	P17	Right-side secondary transverse damper at frame end	49	50	51	2000	50
	P18	Left-side primary suspension at frame end	52	53	54	2000	50
	P19	Right-side primary suspension at frame end	55	56	57	2000	50
	P20	Front-side gearbox at at frame end	58	59	60	2000	50
	P21	Rear-side gearbox at frame end	61	62	63	2000	50
Axle box	P22	Left-side axle box of No.2 wheelset	64	65	66	4000	500
	P23	Right-side axle box of No.2 wheelset	67	68	69	4000	500
Motor	P24	Front-side motor	70	71	72	4000	500
	P25	Rear-side motor	73	74	75	4000	500
Gearbox	P26	Front-side gearbox	76	77	78	4000	500
	P27	Rear-side gearbox	79	80	81	4000	500

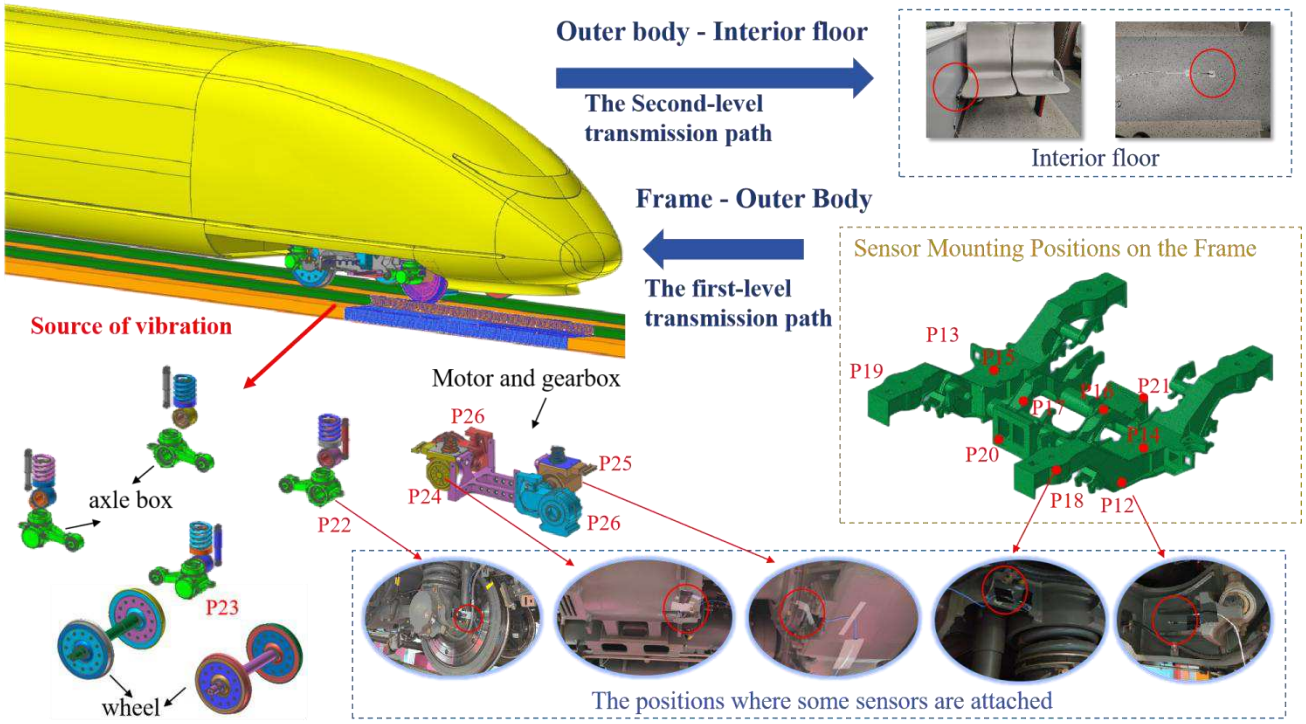

Fig. 2 the vibration transmission paths and the positions of selected acceleration sensor measurement points

Round-trip tests were conducted on the mainline under two operational configurations: with the test vehicle operating as the leading car and as the trailing car. The maximum steady-state running speed of the vehicle was 160 km/h, and the corresponding maximum rotational speed was 996 r/min. In the leading-car configuration, the test included three acceleration-deceleration cycles, whereas the trailing-car configuration followed a single, stable sequence of acceleration, constant-speed operation, and deceleration. The train's operating speed profile and the sampling intervals for representative operating conditions are shown in Fig. 3.

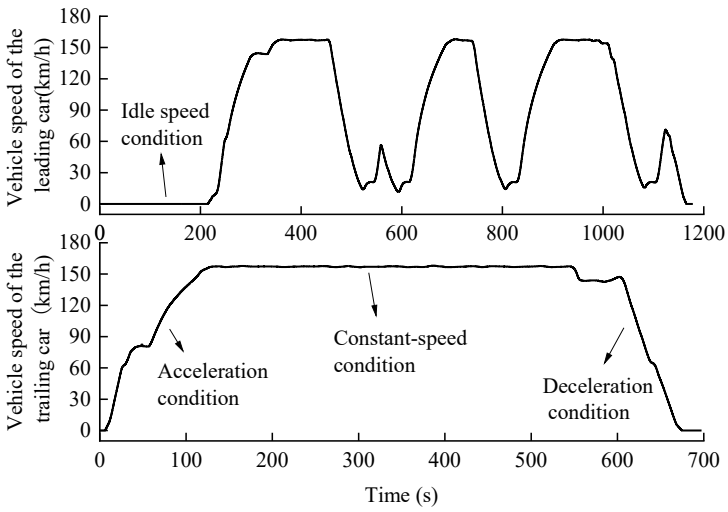

Fig. 3 Train Time-Speed History Diagram

2 Analysis of Train Vibration Laws and Energy Attenuation Characteristics

The field test covered several complete operational round trips. Due to the large number of measurement points, diverse operating conditions, and substantial data volume, it is impractical to present all vibration data in detail. However, by conducting sampled analysis of representative operating conditions and selected key measurement points, the overall vibration characteristics and transmission behavior of the rail vehicle can be comprehensively reflected. The representative operating conditions include acceleration phases, constant-speed operation under leading-car configuration, and constant-speed operation under trailing-car configuration. Given that the vibration levels of the front bogie are typically higher than those of the rear bogie, this study primarily focuses on the first-end bogie and its second axle wheelset. Therefore, the vibration acceleration data presented in the following figures are all based on this configuration.

2.1 Vibration Characteristics Analysis Under Acceleration Conditions

Straight track sections account for approximately 70% to 80% of the total test line length and constitute the primary component of the route. The dynamic behavior of the train on straight sections is representative of the dominant vibration characteristics of the vehicle system. Taking the case where the test vehicle operates as the trailing car on the mainline, as shown in Fig. 3, a 150~240 s segment during the acceleration phase was extracted. The vertical response of the axle box, traction motor, and gearbox under acceleration conditions was analyzed using the short-time Fourier transform (STFT), yielding their time-frequency amplitude spectra, which are presented in Fig. 4.

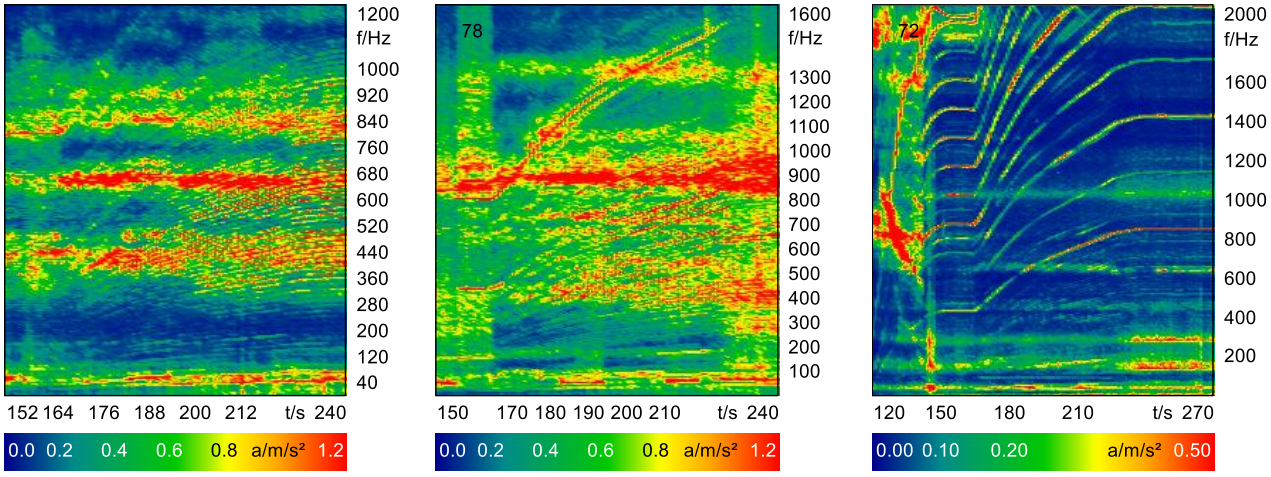

(a) axle box (b) gearbox (c) motor

Fig. 4 Vertical vibration time-frequency diagrams of axle box, gearbox and motor under acceleration condition

When a railway train runs on the rail, numerous frequencies will be generated due to wheel-rail impact. Meanwhile, the vibrations of the bogie frame and car body will also be affected by the characteristic frequencies of the motor and gearbox. According to the vehicle operating speed, the frequencies corresponding to each order of wheel non-roundness excitation can be calculated:

$$f_i = \frac{VN_i}{3.6\pi D} \tag{1}$$

In the formula: V is the vehicle speed, with the unit of km/h; N_i is the wheel polygon order;D is

the wheel rolling circle diameter, which is 0.84m.

The vibration frequency of a railway train is not only related to wheel non-roundness, but also closely related to sleeper spacing[17]. Equation (2) gives the frequency corresponding to sleeper-span impact at a certain speed.

$$f_j = \frac{VN_j}{3.6L} \tag{2}$$

In the formula:N_l is the multiple number; L is the sleeper spacing, approximately 0.59m.

Equations (1) and (2) indicate that the frequency f is proportional to the rotational speed N . Therefore, as shown in Fig. 4(a), multiple red ridges appear on the axle box during the acceleration phase, increasing progressively with vehicle speed. These ridges correspond to the various orders of wheel out-of-roundness and the harmonic frequencies of the sleeper-passing excitation. When the vehicle speed reaches 160 km/h, the measured wheel rotational speed is 996 r/min. According to Eqs. (1) and (2), the corresponding axle rotational frequency is 16.6 Hz, and the sleeper-passing impact frequency is 75.2 Hz.

As shown in Fig. 4(a), increased vibration energy is observed along frequency bands of 40~50 Hz, 360~500Hz, 600~700Hz, and 760~860Hz, accompanied by evident frequency modulation phenomena. At a vehicle speed of 160 km/h, the center frequencies are identified as 414.1 Hz and 646 Hz, with a modulation frequency of 16.6 Hz, corresponding to the axle rotational frequency. This behavior arises from speed-dependent external excitations—such as wheel out-of-roundness—that, as the train accelerates, may align with the natural frequency bands of the wheelset-rotor system, leading to resonance. Consequently, the vibration energy of the associated components is amplified at these frequencies, which is consistent with the findings reported in Ref.[14]. Table 2 summarizes the relationship between the excitation frequencies corresponding to these spectral lines and the natural frequencies of the system components.

As shown in Fig. 4(b), during the acceleration phase, increased vibration levels are observed in the gearbox within the frequency bands of 400~500Hz and 800~1000Hz. At a vehicle speed of 160 km/h, resonance modulation phenomena are identified on the gearbox, with carrier frequencies of 430.7 Hz, 662.1 Hz, and 894.5 Hz, and a modulation frequency of 16.6 Hz corresponding to the axle rotational frequency. These modulated resonances are associated with the excitation of the natural frequencies of the gearbox housing and gear components by external disturbances such as wheel-rail interactions. As indicated in Table 2, the measured peaks at 662.1 Hz and 894.5 Hz are likely related to the second- and fifth-order resonant modes of the gearbox housing, respectively. The dominant peak at 1569 Hz corresponds to the gear meshing frequency, around which sidebands spaced by the axle rotational frequency (16.6 Hz) are clearly observed, forming a modulation sideband structure.

In Fig. 4(c), red ridges that increase with vehicle speed are also present. The large gear in the gearbox has 95 teeth, and the pinion has 22 teeth. At a speed of 160 km/h, the motor rotational frequency is 71.68 Hz. Within the 0-2000Hz frequency range, a series of equally spaced harmonic peaks appear at integer multiples of the motor rotational frequency. Prominent peaks are observed at 142.6 Hz, 286.1 Hz, 858.4 Hz, and 1432 Hz, corresponding to the 2nd, 4th, 12th, and 20th harmonics of the motor rotational frequency, respectively.

Tab 2 The relationship between the excitation frequency corresponding to the lines and the natural frequency of system components

Wheel Set	Bogie Frame	Gearbox

Order	Natural Frequency/Hz	Order	Natural Frequency/Hz	Order	Natural Frequency/Hz
1	97.19	1	42.07	1	594
2	102.38	2	68.94	2	660
12	420.01	3	86.18	3	665
21	629.32	4	87.73	6	890

2.2 Vibration Characteristics Analysis Under Constant-Speed Condition

As shown in Fig. 3, constant-speed operating segments were extracted from the test data: 940~1000s when the test vehicle operated as the leading car, and 140~200s when it operated as the trailing car. The time-domain and frequency-domain characteristics of the axle box, bogie frame, and carbody vibrations were analyzed, with the bogie frame vibration represented by measurements taken at the frame-side end of the primary suspension. Figure 4 presents the time histories of the vehicle's vibration accelerations. It can be observed that the vertical vibration accelerations are generally higher than the lateral components, particularly at the axle box. The vibration acceleration of the interior floor is primarily within the range of $\pm 1.5\ m/s^2$, while that of the bogie frame ranges between $\pm 30\ m/s^2$. The lateral acceleration of the axle box varies within $\pm 80\ m/s^2$, and the vertical acceleration reaches up to $\pm 150\ m/s^2$. From a time-domain perspective, the vibration amplitudes under the leading-car and trailing-car configurations are comparable, with no significant difference in magnitude.

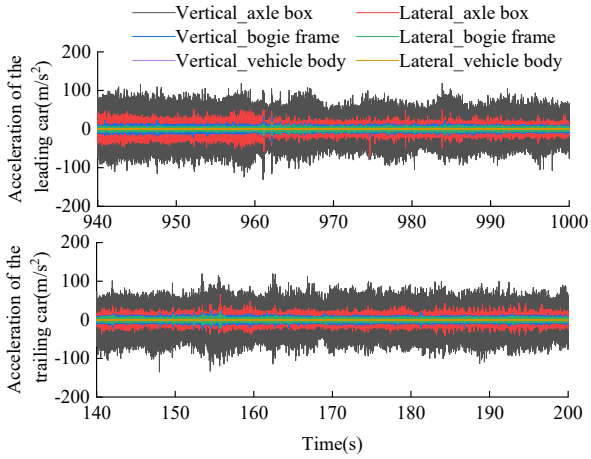

Fig. 5 Time-domain Diagram of Vehicle Vibration Acceleration Under Constant-Speed Condition

Figures 6, show the power spectral density (PSD) of vibration acceleration at the front end of the carbody, the axle box, and the bogie frame, respectively, under both leading-car and trailing-car operating conditions.

As shown in Fig.6(a), distinct vibration peaks are observed at the front end of the carbody at frequencies of 1.83 Hz, 16.6 Hz, 71.53 Hz, and 143.12 Hz. These peaks correspond to the carbody's rigid-body mode, the axle rotational frequency, the traction motor rotational frequency, and the second-order electromagnetic harmonic of the traction motor, respectively. In the low-frequency range (0~20 Hz), the carbody vibration under the trailing-car condition is significantly higher than that under the leading-car condition, with the peak at 1.83 Hz being particularly prominent. This is attributed to the fact that, as the last vehicle in the train formation, the trailing car lacks the longitudinal and lateral constraint provided by subsequent vehicles, resulting in larger lateral displacements of the wheelsets and increased low-frequency carbody response. In the mid-to-high frequency range (40~160 Hz), the vertical carbody vibration is influenced by track irregularities, motor-induced excitations, and

aerodynamic forces. The vibration level under the leading-car condition exceeds that under the trailing-car condition in this band. This is primarily due to greater aerodynamic pressure fluctuations acting on the leading car during high-speed operation. Flow separation around the nose fairing and bogie region can generate vortex-induced vibrations in the 120~150 Hz range at certain speeds, which may couple with local flexible modes of the carbody front structure, leading to amplified vibration responses.

As shown in Fig. 6(b), the dominant vibration of the axle box occurs in the frequency bands of 300~500 Hz, 600~700 Hz, and 800~1000 Hz, with vertical acceleration significantly exceeding lateral acceleration. In the 300~500 Hz range, the vibration energy under the leading-car condition is higher than that under the trailing-car condition, with particularly prominent peaks at 396.48 Hz, 429.5 Hz, and 446 Hz. These frequencies correspond to the 24th, 26th, and 27th harmonics of the axle rotational frequency, respectively, and are associated with the wavelength components of track irregularities. High-frequency vibrations above 1000 Hz exhibit low energy levels, indicating that wheel-rail excitation typically induces axle box vibrations below 1000 Hz. Under the leading-car condition, the root mean square (RMS) values of lateral and vertical axle box accelerations are 4.03 m/s^2 and 23.91 m/s^2, respectively, compared to 3.90 m/s^2 and 24.04 m/s^2 under the trailing-car condition. The slightly higher lateral vibration under the leading-car condition suggests a greater influence of aerodynamic effects on lateral axle box dynamics.

As shown in Fig.6(c), the vibration of the bogie frame is predominantly concentrated in the low-frequency range of 0~80Hz. Within this band, the vibration levels under the trailing-car condition are significantly higher than those under the leading-car condition, for both vertical and lateral directions. The dominant vibration frequency is 49.68 Hz, which corresponds to the third harmonic of the axle rotational frequency. In the vertical spectrum, peaks at 66.22 Hz, 75.19 Hz, and 143.7 Hz are identified as the fourth harmonic of the axle rotation, the sleeper-passing frequency, and the motor rotational frequency, respectively. The periodic excitation induced by wheel rotation is not effectively attenuated by the primary suspension system, leading to transmission of these vibrations to the bogie frame and resulting in resonant responses at the same frequencies. At the peak frequency of 143.7 Hz, the vertical vibration amplitude of the frame under the leading-car condition is considerably greater than that under the trailing-car condition, which can be attributed to the combined effects of aerodynamic pressure fluctuations and motor-induced excitations in the leading car.

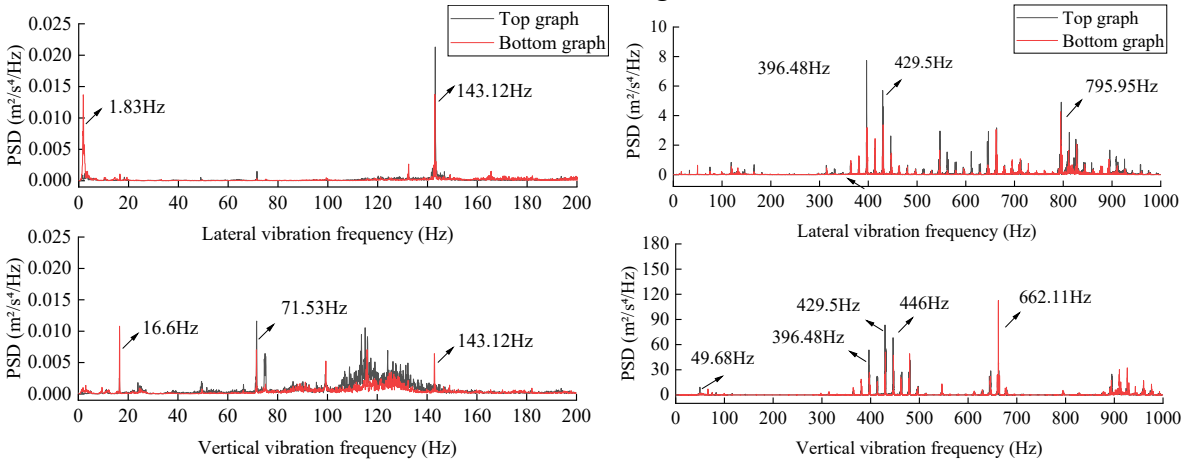

(a) Front End of Car Body (b) Axle Box

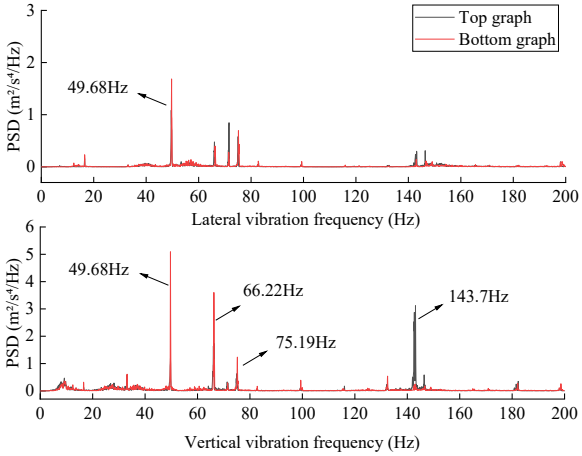

(c) Bogie Frame

Fig. 6 PSD of Vibration Acceleration of vehicle

2.3 Analysis of Train Vibration Energy Attenuation Characteristics

To provide a more intuitive assessment of the influence of wheel-rail excitation on train vibration, the measurements from all sensor points on the carbody, bogie frame, and axle box under both leading-car and trailing-car conditions were first averaged and then subjected to statistical analysis.

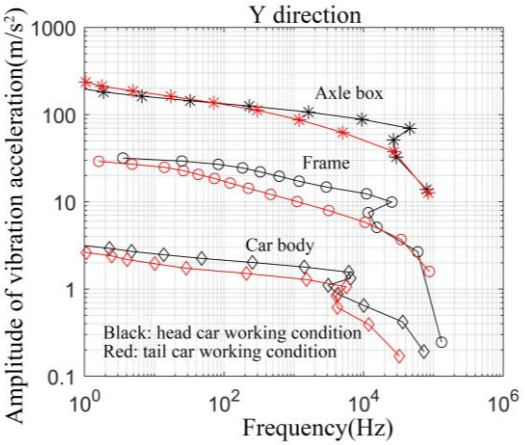

Fig. 7 Lateral Vibration Amplitude-Frequency Diagram

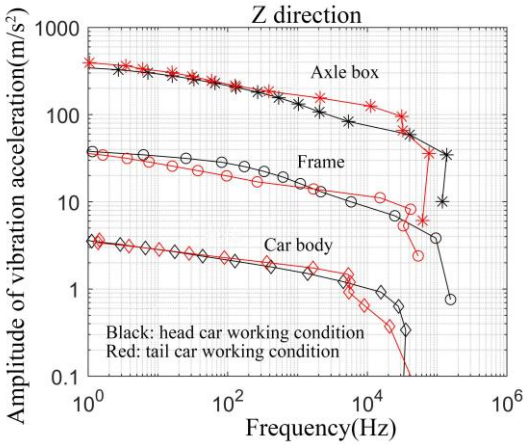

Fig. 8 Vertical Vibration Amplitude-Frequency Diagram

As shown in Figs. 7 and 8, the maximum vibration amplitudes of the axle box, bogie frame, and carbody fall within the ranges of 250~450m/s² , 30~40m/s² , and 3~4 m/s² , respectively. Acceleration peaks with relatively high magnitudes but low occurrence frequency are primarily induced by track irregularities such as turnouts and rail joints. In contrast, the more frequent but smaller-amplitude vibrations are associated with operational conditions such as acceleration and deceleration, as well as excitations caused by continuous track irregularities.

Due to the lack of synchronized speed profiles between the leading-car and trailing-car test runs, a direct comparison of vibration levels based solely on vehicle speed is not feasible. Taking the trailing-car condition as an example, the root mean square (RMS) values of lateral and vertical vibration accelerations at carbody measurement points are 0.27 m/s² and 0.22 m/s² , respectively; those at the bogie frame are 2.45 m/s² (lateral) and 3.07 m/s² (vertical); and those at the axle box are 7.68 m/s² (lateral) and 16.78 m/s² (vertical). The vibration transmission from the axle box to the bogie frame

exhibits more pronounced attenuation in the vertical direction. Further, as vibration propagates from the bogie frame to the carbody, the overall attenuation ratio is approximately 0.1.

3 Vibration Transfer Path Analysis

3.1 Theoretical Analysis of OTPA

In the process of transfer path analysis, the vibration at the target point is obtained by the linear superposition of vibrations from the excitation point along each transfer path to the target point. The vibration transfer characteristics of the system can be expressed as:

$$\mathbf{Y} = \mathbf{XT} \tag{3}$$

In the formula: $\mathbf{X}$ is the system input matrix; $\mathbf{Y}$ is the output matrix; $\mathbf{T}$ is the transfer function matrix. In order to solve the matrix $\mathbf{T}$, m tests need to be conducted, then Equation (3) can be written as:

$$\begin{bmatrix} Y_{11} & Y_{21} & \cdots & Y_{c1} \\ Y_{12} & Y_{22} & \cdots & Y_{c2} \\ \vdots & \vdots & \ddots & \vdots \\ Y_{1m} & Y_{2m} & \cdots & Y_{cm} \end{bmatrix} = \begin{bmatrix} X_{11} & X_{21} & \cdots & X_{n1} \\ X_{12} & X_{22} & \cdots & X_{n2} \\ \vdots & \vdots & \ddots & \vdots \\ X_{1m} & X_{2m} & \cdots & X_{nm} \end{bmatrix} \begin{bmatrix} T_{11} & T_{12} & \cdots & T_{1c} \\ T_{21} & T_{22} & \cdots & T_{2c} \\ \vdots & \vdots & \ddots & \vdots \\ T_{n1} & T_{n2} & \cdots & T_{nc} \end{bmatrix} \tag{4}$$

In the formula: X_{nm} is the n-th input of the system measured under the m-th test condition; Y_{cm} is the c-th output of the system measured under the m-th test condition; T_{nc} is the path transfer function from the n-th input at the excitation point to the c-th output at the target point. Generally, it is required that m is more than twice n.

In order to avoid the mutual interference between input signals affecting the calculation accuracy, by using singular value decomposition on the input signals of the working-condition data, a series of linearly independent principal-component vectors are obtained, thus forming the principal-component space. The core of this method is performing singular value decomposition on the input matrix, which can be expressed as:

$$\mathbf{X} = \mathbf{UDV}^{\mathrm{T}} \tag{5}$$

$$\mathbf{D} = \begin{bmatrix} \sigma_1 & 0 & \cdots & 0 \\ 0 & \sigma_2 & \cdots & 0 \\ \vdots & \vdots & \ddots & \vdots \\ 0 & 0 & \cdots & \sigma_n \\ \vdots & \vdots & \vdots & \vdots \\ 0 & 0 & 0 & 0 \end{bmatrix} \tag{6}$$

In the formula: $\mathbf{U}$ and $\mathbf{V}$ are the left and right singular matrices of $\mathbf{X}$, both of which are unitary matrices; $\mathbf{D}$ is the singular-value matrix of $\mathbf{X}$, which is an m$\times$n diagonal matrix. The value σ_i (i$\leq$n) on its diagonal is the singular value of $\mathbf{X}$. Larger singular values correspond to the main components in the input signal, while smaller singular values correspond to the secondary components in the input signal. Reasonably discarding smaller singular values can reduce the influence of measurement noise on the calculation of the transfer function. According to the excitation source and transfer function, the contribution of each path can be obtained.

3.2 Two-stage OTPA Vibration Transfer Path Analysis

A two-stage transfer path analysis model was established, consisting of the paths “external carbody—interior floor” (Stage 1) and “bogie frame—external carbody” (Stage 2), as illustrated in Fig. 9. In the first stage, the vertical vibrations of the front-end floor, seat, and central floor inside the carbody were selected as response points, while the carbody-side ends of the secondary suspension components and the connection points between the traction inverter and the carbody were treated as excitation sources. In the second stage, the lateral and vertical vibrations at the carbody-side ends of the right-side anti-yaw damper, left-side anti-roll torsion bar, and center pin were used as response points, and the measurements from the corresponding locations on the bogie frame were taken as excitation sources. The contribution of each excitation source to the respective response points was analyzed to identify the dominant vibration transmission paths. The measurement point locations corresponding to each channel are listed in Table 1.

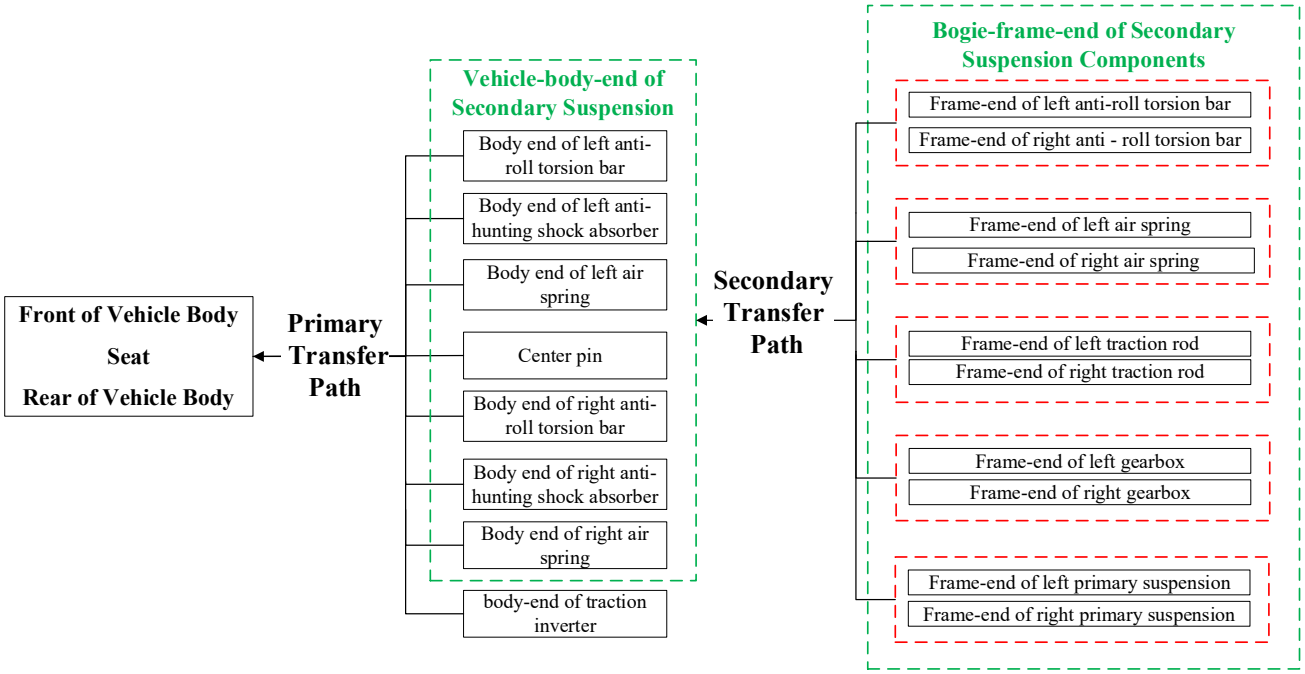

Fig. 9 Schematic Diagram of Two-Stage Transfer Path

To validate the accuracy of the Operational Transfer Path Analysis (OTPA) model, a model validation procedure was conducted. As shown in Fig. 3, the two-stage OTPA vibration transmission model was established using vibration data from the trailing-car condition. Subsequently, data from the leading-car constant-speed condition (940~1000 s) were used as an independent validation set to assess the accuracy of all nine OTPA paths—three response points in the first stage and six in the second stage. The validation results are presented in Fig.10, where the green lines represent the measured responses from the validation set, and the red lines denote the OTPA-predicted responses. As shown, the measured and predicted responses exhibit good agreement in both peak amplitudes and overall vibration trends, confirming the accuracy and reliability of the established OTPA model.

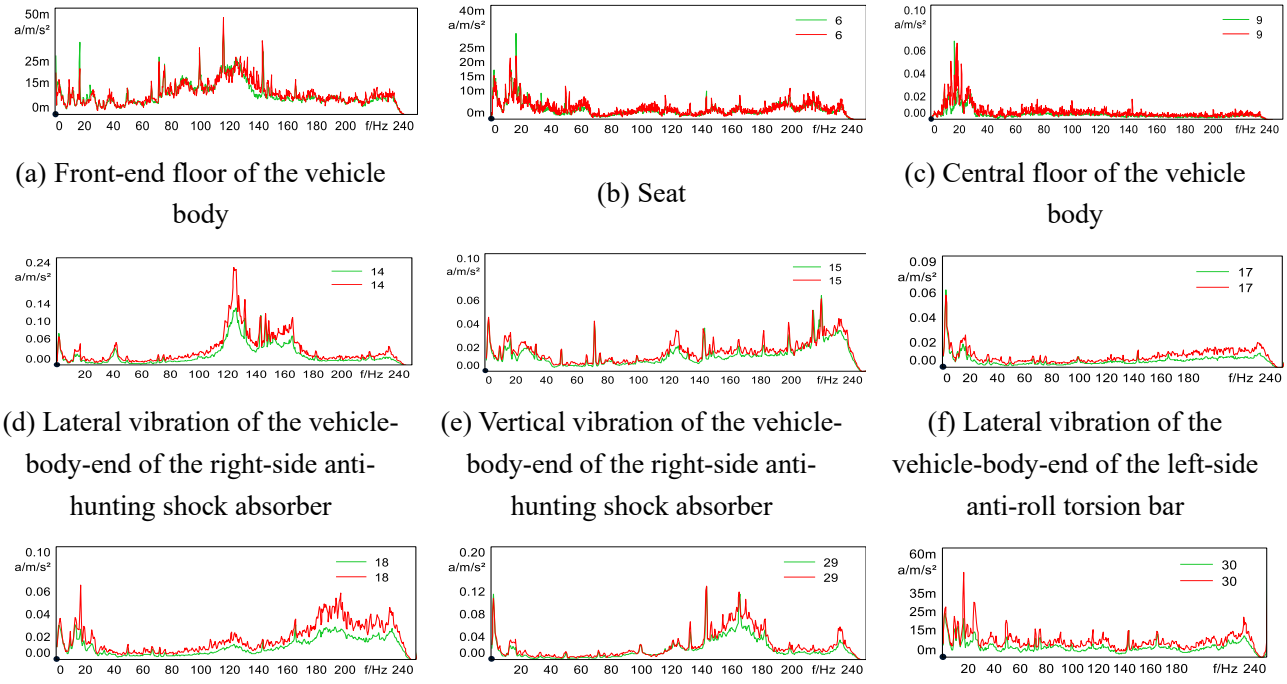

(a) Front-end floor of the vehicle body

(b) Seat

(c) Central floor of the vehicle body

(d) Lateral vibration of the vehicle-body-end of the right-side anti-hunting shock absorber

(e) Vertical vibration of the vehicle-body-end of the right-side anti-hunting shock absorber

(f) Lateral vibration of the vehicle-body-end of the left-side anti-roll torsion bar

(g) Vertical vibration of the vehicle-body-end of the left-side anti-roll torsion bar

(h) Lateral vibration of the center pin

(g) Vertical vibration of the center pin

Fig10. Verification of the OTPA Model

3.3 Establishment and Analysis of the OTPA Model for the "Outer Vehicle Body-Interior Vehicle Floor" System

As indicated by the above analysis, the vertical vibration amplitude of the carbody is greater than the lateral component. Therefore, in analyzing the vibration transmission path from the external carbody to the interior floor, three OTPA models were established with the vertical vibrations of the front-end floor, seat, and central floor as response points. Figure 13 presents the contribution of each excitation source on the external carbody to these response points across the frequency spectrum. In Figs.11(a), 10(b), and 10(c), the first column in each subplot represents the measured response at the front-end floor, seat, and central floor, respectively, while the remaining 24 columns correspond to the contribution levels of the external carbody excitation sources within specific frequency bands. The channel definitions are provided in Table 1. In the figure, the intensity of the color indicates the magnitude of the contribution: warmer colors (red) represent higher contributions, while cooler colors (blue) indicate lower contributions.

Overall, in the frequency range of 60~200 Hz, the blocks corresponding to paths 13, 14, 15, 28, and 29exhibit the highest intensity, indicating significant contribution. This suggests that mid-to-high-frequency vibrations are primarily transmitted to the interior floor via the carbody-side ends of the anti-yaw dampers and the center pin. In the mid-to-low frequency range, a distinct peak is observed at 16.6 Hz in the interior floor responses. Table 3 lists the ranking of contribution levels from various excitation sources to the response points at this peak frequency. As shown, for all three response locations—front-end floor, seat, and central floor—the highest contribution comes from Channel 28, which corresponds to the longitudinal direction of the center pin. This indicates that the periodic excitation induced by wheel rotation at the axle rotational frequency is transmitted upward to the bogie

frame and subsequently propagated to the carbody interior primarily through the center pin.

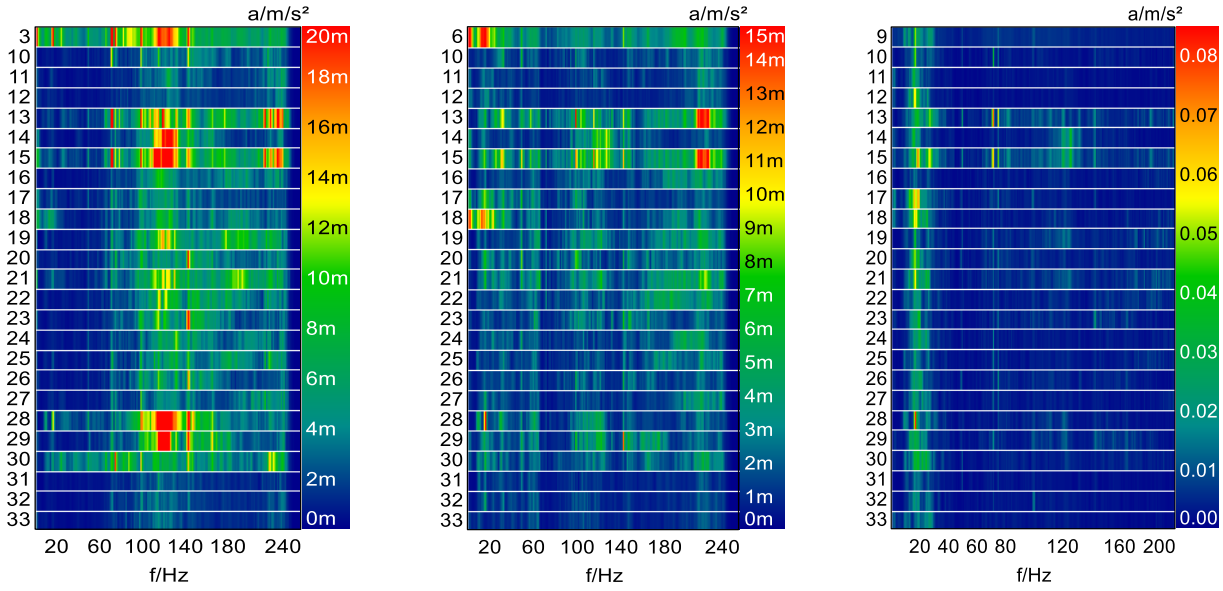

(a) Vertical vibration of the front-end floor of the vehicle body

(b) Vertical vibration of the seat

(c) Vertical vibration of the central floor of the vehicle body

Fig11. Diagram of the contribution of each excitation source in the first-level transfer path to the response points

Tab3. Ranking table of the contribution of each excitation source at the peak frequency of 16.6 Hz

Vertical Vibration of the Front-end Floor of the Vehicle Body		Vertical Vibration of the Seat		Vertical Vibration of the Central Floor of the Vehicle Body	
Channel	Contribution (m/s²)	Channel	Contribution (m/s²)	Channel	Contribution (m/s²)
28	0.01742	28	0.02260	28	0.10208
30	0.00764	18	0.01228	21	0.07891
18	0.00706	17	0.01036	12	0.07225
21	0.00626	21	0.00974	10	0.07185
25	0.00364	20	0.00929	20	0.06863
29	0.00338	13	0.00890	17	0.05687

3.4 Establishment and Analysis of the OTPA Model for the "Bogie Frame-Outer Vehicle Body"

As indicated by the above analysis, the center pin, the carbody-side ends of the anti-yaw dampers, and the anti-roll torsion bars contribute to the vertical vibration of the interior floor and seat to varying degrees. Therefore, in establishing the second-stage OTPA model for the transfer path from the bogie frame to the external carbody, six response points were selected: the lateral and vertical vibrations at the carbody-side end of the right-side anti-yaw damper, the lateral and vertical vibrations at the carbody-side end of the left-side anti-roll torsion bar, and the lateral and vertical vibrations at the center pin. The measurement points at the frame-side ends of the secondary suspension components were used as excitation sources. This configuration results in six OTPA models and a total of 30 transfer paths.

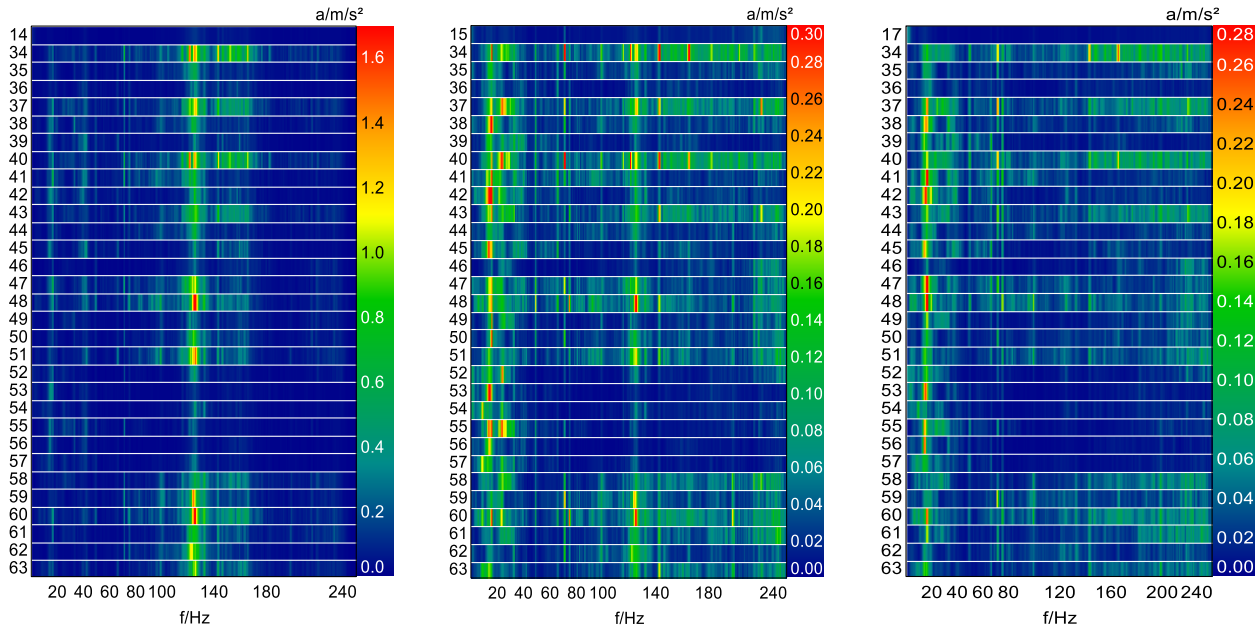

(a) Lateral Vibration of Vehicle-body-end of Right-side Anti-hunting Shock Absorber

(b) Vertical Vibration of Vehicle-body-end of Right-side Anti-hunting Shock Absorber

(c) Lateral Vibration of Vehicle-body-end of Left-side Anti-roll Torsion Bar

(d) Vertical Vibration of Vehicle-body-end of Left-side Anti-roll Torsion Bar

(e) Lateral Vibration of Center Pin

(f) Vertical Vibration of Center Pin

Fig12. The Contribution of Each Excitation Source to the Response Points in the Second-level Transfer Path

Figure 12 presents the contribution matrix of excitation sources to the response points in the second-stage transfer path. Overall, in the mid-to-high frequency range of 40~250 Hz, the color intensity of channels 52~57 is relatively low, indicating minimal contribution. This suggests that the connection points between the primary suspension and the bogie frame have limited influence on the

response points in the second-stage transmission path. In contrast, other channels exhibit varying degrees of contribution. To enable a more quantitative assessment of the overall contribution of each channel to the six response points across the 0~250 Hz frequency range, the root mean square (RMS) of the contribution levels was calculated. The results are shown in Fig. 13.

As shown in Fig. 13, the average contribution level to the lateral vibration at the carbody-side end of the right-side anti-yaw damper is higher than those to the other five response points. When the lateral and vertical vibrations at the left-side anti-roll torsion bar carbody end and the center pin are considered as response points, channels 34 and 40 exhibit relatively high contributions. For the lateral and vertical responses at the right-side anti-yaw damper carbody end, significant contributions are observed from channels 34, 37, 40, 48, 51, and 60. These channels correspond to the longitudinal direction at the frame-side ends of the left-side anti-yaw damper/anti-roll bar, the right-side anti-yaw damper/anti-roll bar, the left-side air spring/vertical damper, the vertical direction at the frame-side end of the left-side secondary lateral damper, the right-side secondary lateral damper, and the vertical direction at the front-side gearbox frame end, respectively.

The frame-side connection points of the anti-yaw dampers, anti-roll bars, air springs, and vertical dampers are located on the mid-span region of the bogie side beams, while the measurement points for the secondary lateral dampers and the gearbox are situated on the cross beam of the bogie frame. The results indicate that vibration is primarily transmitted from the central region of the side beams to the carbody-side ends of the anti-roll torsion bar and the center pin.

As can be seen from Fig. 12(a), at the dominant excitation frequency of 126 Hz, the blocks corresponding to Channels 48, 51, and 60 exhibit a redder color, indicating higher contribution levels. Combining the contribution values at this characteristic frequency with the overall RMS contribution across the frequency band, it can be concluded that vibration is primarily transmitted from the mid-span region of the bogie side beams and the cross beam to the carbody-side ends of the anti-yaw dampers.

Tab4 Ranking Table of the Contribution of Each Excitation Source in the Second-level Transfer Path at the Peak Frequency of 16.6 Hz

Lateral Vibration of Vehicle-body-end of Right-side Anti-hunting Shock Absorber		Vertical Vibration of Vehicle-body-end of Right-side Anti-hunting Shock Absorber		Lateral Vibration of Vehicle-body-end of Left-side Anti-roll Torsion Bar		Vertical Vibration of Vehicle-body-end of Left-side Anti-roll Torsion Bar		Lateral Vibration of Center Pin		Vertical Vibration of Center Pin	
Channel	Contribution (m/s^2)	Channel	Contribution (m/s^2)	Channel	Contribution (m/s^2)	Channel	Contribution (m/s^2)	Channel	Contribution (m/s^2)	Channel	Contribution (m/s^2)
41	0.75333	38	0.63995	47	0.42993	47	1.14674	41	0.64490	38	0.71425
47	0.71460	60	0.40117	48	0.42428	41	0.97774	47	0.63234	47	0.61260
48	0.51227	50	0.39149	41	0.38337	38	0.63660	48	0.46152	42	0.45980
37	0.51055	41	0.37583	60	0.32719	42	0.62400	60	0.44946	48	0.36919
60	0.50310	34	0.37396	37	0.31981	44	0.54791	37	0.40135	60	0.36281
40	0.49824	42	0.36419	38	0.28041	35	0.50504	40	0.37806	41	0.35986

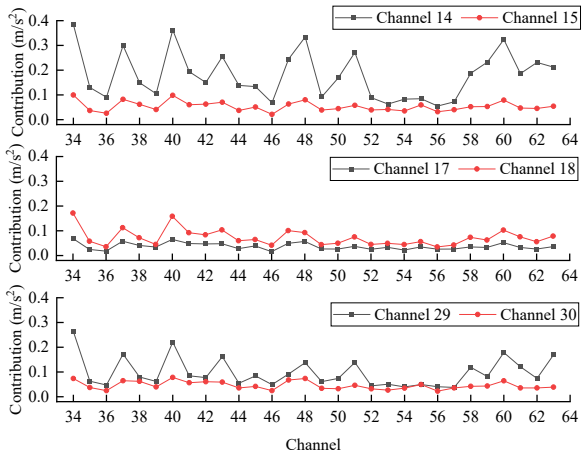

Fig13. The Comprehensive Value of the Contribution Quantity

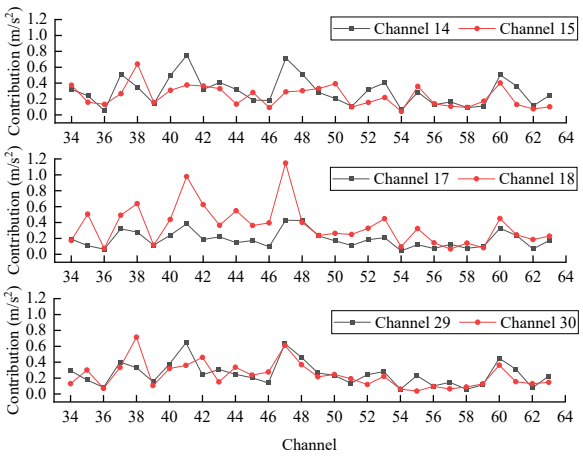

Fig14. The Contribution Quantity at the Frequency of 16.6 Hz

As shown in Fig.12, a distinct peak frequency at 16.6 Hz is present in all response points. Figure 15 presents the contribution of each excitation source in the second-stage transfer path at this peak frequency. The top six contributing channels and their corresponding contribution values are listed in Table 4. It can be observed that, for the vertical vibrations at the carbody-side end of the right-side anti-yaw damper and the center pin, Channel 38—corresponding to the lateral direction at the frame-side end of the right-side anti-yaw damper/anti-roll torsion bar—exhibits the highest contribution. For the lateral vibrations at these same locations, Channel 41—the lateral direction at the frame-side end of the left-side air spring/vertical damper—shows the largest contribution. For the lateral and vertical responses at the carbody-side end of the left-side anti-roll torsion bar, the dominant contribution comes from Channel 47, which corresponds to the lateral direction at the frame-side end of the left-side secondary lateral damper. Therefore, the excitation induced by wheel out-of-roundness is primarily transmitted from the mid-span region of the bogie side beams to the external carbody.

3.5 Transfer Function Analysis of the "Axle Box-Bogie Frame" System

As shown in Fig.3, constant-speed data from the trailing-car condition (300~600s) were selected to analyze the vibration transmission characteristics of the primary suspension. The frequency response functions (FRFs) from the axle box to the frame-side ends of the primary suspension, gearbox, secondary lateral damper, anti-yaw damper, and air spring were calculated using the Fast Fourier Transform (FFT) method. The longitudinal, lateral, and vertical transfer characteristics of these paths are presented in Figs. 15~17.

As can be seen from Figs.15~17, the transfer functions from the axle box to the bogie frame are generally below unity across most of the frequency range, except for several localized bands. This indicates that vibrations induced by wheel-rail excitations are effectively attenuated during transmission from the axle box to the frame, with the most significant attenuation observed for mid-to-high frequency components above 300 Hz. Overall, the highest transmissibility is observed in the path from the axle box to the frame-side end of the primary suspension, with peak values reaching 6.2 in the longitudinal direction, 2.4 in the lateral direction, and 3.9 in the vertical direction. This suggests that the primary suspension springs and the primary vertical dampers constitute the dominant paths for vibration energy transmission within the primary suspension system.

In the 600~700 Hz frequency band, the transmissibility from the axle box to the gearbox frame end is slightly higher than that of other paths. This transmission characteristic is likely closely associated with the dynamic behavior of the traction motor, gearbox, and coupling system.

In the 0~300Hz range, four peak frequencies are observed at 2 Hz, 59.8 Hz, 219.9 Hz, and 285.5 Hz. The peak at 2 Hz is related to the yaw motion of the bogie frame, while the other peaks correspond to different modal orders of the frame structure. Wheel-rail excitation induces resonance in the bogie frame, leading to amplified vibration transmission from the axle box to the frame at these frequencies.

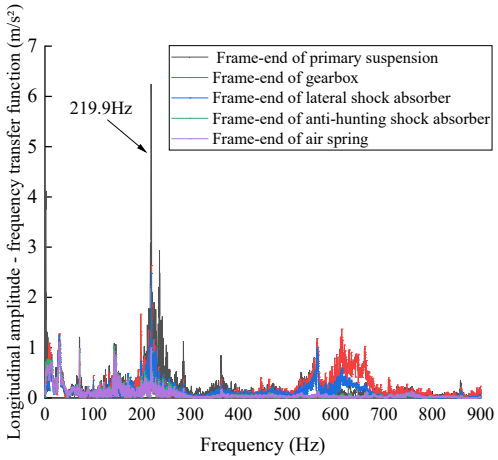

Fig15. The Longitudinal Transfer Coefficient from the Axle Box to the Bogie Frame

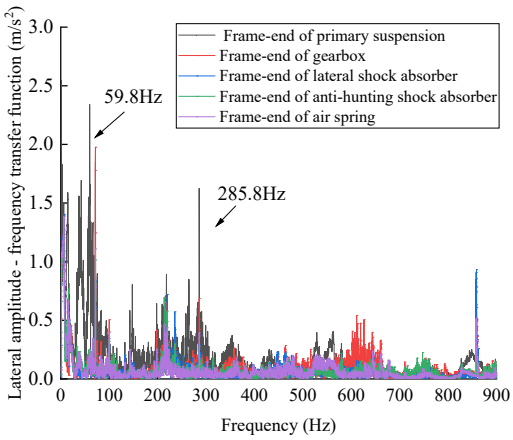

Fig16. The Lateral Transfer Coefficient from the Axle Box to the Bogie Frame

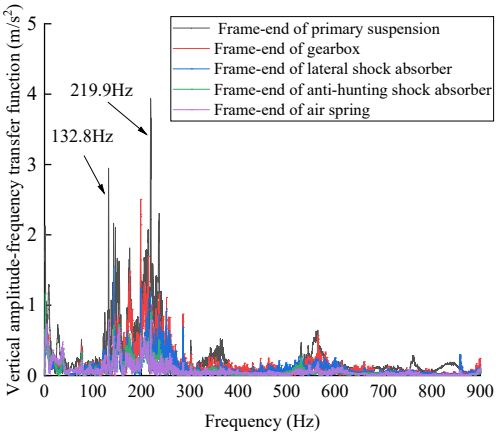

Fig17. The Vertical Transfer Coefficient from the Axle Box to the Bogie Frame

In summary, wheel-rail excitations induced by track irregularities and wheel out-of-roundness are transmitted from the axle box to the frame-side ends of the primary suspension, then propagated through the mid-span region of the bogie side beams and the cross beam, and finally channeled primarily through the anti-yaw dampers and center pin to the carbody interior.

4 Conclusions

Vibration acceleration signals were acquired from key components of a rail vehicle, including the axle boxes, traction motors, gearboxes, bogie frames, and carbody, through field testing. Based on the

analysis of these data, the following conclusions regarding the vehicle's time–frequency response, energy attenuation characteristics, and vibration transmission paths are drawn:

1. Distinct frequency modulation phenomena are observed in the vibration characteristics of the axle box, gearbox, and traction motor. In their time-frequency representations, ridge patterns resembling the speed-time profile are identified, which correspond to various orders of wheel out-of-roundness, sleeper spacing, motor rotational harmonics, and gear meshing frequencies of the pinion and large gear. During acceleration, as the vehicle speed increases, the frequencies of periodic external excitations rise accordingly. When these excitation frequencies align with the natural frequency bands of certain system components, the vibration energy at those frequencies is amplified due to resonance.

2. Under constant-speed operation with the test vehicle configured as both the leading and trailing car, the vibration characteristics of the axle box, bogie frame, and carbody are analyzed in both the time and frequency domains. The effective vibration frequencies induced by various track and wheel irregularities are generally below 1000 Hz, while the dominant vibrations of the frame and carbody are concentrated within 200 Hz. Due to the absence of trailing vehicles'constraint at the rear of the train, the wheelsets in the trailing car experience larger lateral displacements, resulting in significantly higher carbody vibration levels under the trailing-car condition in the 0~20Hz low-frequency range, particularly at 1.83Hz. In contrast, under the leading-car condition, the combined effects of aerodynamic pressure fluctuations, track irregularities, and motor-induced excitations lead to higher carbody vibration levels in the 40~160 Hz mid-to-high frequency range.

3. The vertical vibration acceleration of the axle box is considerably higher than the lateral component. Statistical analysis of measurement data from the axle box, bogie frame, and carbody reveals that vibration is attenuated by approximately one order of magnitude as it propagates from the axle box to the carbody via the bogie frame. The most significant attenuation occurs in the vertical direction during transmission from the axle box to the frame.

4. A two-stage transfer path model was established, consisting of the paths "external carbody—interior floor" and "bogie frame—center pin". Through analysis of the transmissibility from the axle box to the frame and the two-stage operational transfer path analysis (OTPA), it is determined that excitations caused by wheel out-of-roundness and track irregularities are primarily transmitted through the primary suspension springs and vertical dampers, propagating along the mid-span region of the side beams and the cross beam of the bogie frame, and ultimately channeled to the carbody interior via the anti-yaw dampers and center pin.

Data availability

The datasets generated and/or analysed during the current study are available from the corresponding author on reasonable request.

CRediT authorship contribution statement

Yuqi Cheng: Writing-original draft, Methodology, Data curation. **Qian Xiao:**Funding acquisition, Method Guidance. **Chao Chang:**data processing. **Hesheng Liu:**Method Guidance. **Huanhuan Li:**Method Guidance. **Hu Zeng:**Funding acquisition, Method Guidance.

Declaration of Competing Interest

The authors declare that they have no known competing financial interests or personal relationships that could have appeared to influence the work reported in this paper.

Funding

This work was supported by the National Natural Science Foundation of China (Grant No. 52372327), the Jiangxi Provincial Natural Science Foundation (Grant No. 20242BAB26065), and the Science and Technology Research Projects of the Jiangxi Provincial Department of Education (Grant Nos. GJJ2406911 and GJJ2406909).

References

[1] Bosso, N., Bracciali, A., Megna, G., & Zampieri, N. (2023). Effects of geometric track irregularities on vehicle dynamic behaviour when running through a turnout. Vehicle System Dynamics, 61(3), 782-798.

[2] Zhai, W., Han, Z., Chen, Z., Ling, L., & Zhu, S. (2019). Train-track-bridge dynamic interaction: a state-of-the-art review. Vehicle System Dynamics, 57(7), 984-1027.

[3] Zhai, W. (2019). Numerical method and computer simulation for analysis of vehicle-track coupled dynamics. In Vehicle-Track Coupled Dynamics: Theory and Applications (pp. 203-229). Singapore: Springer Singapore.

[4] Thompson, D. J., Latorre Iglesias, E., Liu, X., Zhu, J., & Hu, Z. (2015). Recent developments in the prediction and control of aerodynamic noise from high-speed trains. International Journal of Rail Transportation, 3(3), 119-150.

[5] Shi, Y., Mao, Q., Dai, H., Wang, Q., & Qi, Y. (2025). Research on abnormal vibration of high-speed train based on wheel-rail coupling modal analysis. Vehicle System Dynamics, 63(3), 457-474.

[6] Wei, L., Zeng, J., Chi, M., & Wang, J. (2017). Carbody elastic vibrations of high-speed vehicles caused by bogie hunting instability. Vehicle System Dynamics, 55(9), 1321-1342.

[7] Qi, Y., Dai, H., Song, C., & Qu, S. (2019). Shaking analysis of high-speed train's carbody when cross lines. Journal of Mechanical Science and Technology, 33(3), 1055-1064.

[8] Ai, Y., Ma, H., Qu, X., Qian, Y., Liu, Y., & Zhang, W. (2022). The Cross-Scale Life Prediction for the High-Speed Train Gearbox Shell Based on the Three-Interval Method. Scientific Programming, 2022(1), 6439229.

[9] Hu, W., Liu, Z., Liu, D., & Hai, X. (2017). Fatigue failure analysis of high speed train gearbox housings. Engineering Failure Analysis, 73, 57-71.

[10] Guo, J., Shi, H., Li, F., & Wu, P. (2020). Field Measurements of Vibration on the Car Body-Suspended Equipment for High-Speed Rail Vehicles. Shock and Vibration, 2020(1), 6041543.

[11] Sun, Q., Chen, C., & Liu, X. (2023). Comparative study of stator current-based and vibration-based methods for railway traction motor bearing cage fault diagnosis at high-speed condition. Structural Health Monitoring, 22(2), 978-992.

[12] Lin Fengtao, Wan Shengyang, Hu Weihao, Liu Baochen, Zhang Hai, Yang Yang. Influence of Wheel Polygon Amplitude on Vibration Transmission Characteristics of Lateral Passing Turnout Area. Machine Tool & Hydraulics, 49(7), 128-134.

[13] Shi, H. L., Qu, S., Zhang, D. F., & Wang, J. (2019). Dynamic response performance analysis of high-speed trains on track. Journal of the China Railway Society, 41(10), 30-37.

[14] Xu, N., Ren, Z., & Xue, R. (2019). Time and frequency domain response and vibration transfer characteristics of high-speed EMU. Journal of the China railway society, 41, 31-40.

[15] Tan, J. J., Chaigne, A., & Acri, A. (2018). Operational transfer path analysis of a piano. Applied Acoustics, 140, 39-47.

[16] Liu, Z., Gao, Y., Yang, J., Xu, X., Fang, J., Duan, Y., & Ma, C. (2021). Transfer path analysis and its application to diagnosis for low-frequency transient vibration in the automotive door slamming event. Measurement, 183, 109896.

[17] Li, M., Liu, Q., Dai, G., Chen, W., & Zhu, R. (2021). Vibration transfer path analysis of double-layer box for marine reducer. Journal of Vibration Engineering & Technologies, 9(6), 1077-1089.

[18] Qin, Y., Wang, Z., Yuan, K., & Zhang, Y. (2019). Comprehensive analysis and optimization of dynamic vibration-absorbing structures for electric vehicles driven by in-wheel motors. Automotive Innovation, 2(4), 254-262.

[19] Liu, C., Zhang, Y. H., Zhang, X. Z., Zhang, Y. B., & Chen, L. Q. (2023). Source contribution analysis of vehicle pass-by noise using a moving multi-band model based OPAX method. Measurement, 218, 113170.

[20] Liu, L., Liang, X., & Zuo, M. J. (2016). Vibration signal modeling of a planetary gear set with transmission path effect analysis. Measurement, 85, 20-31.

[21] Park, U., & Kang, Y. J. (2024). Operational transfer path analysis based on neural network. Journal of Sound and Vibration, 579, 118364.

[22] Yang, W., Chen, J., Liu, Z., & Lan, F. (2019). Vibration characteristics of framed suv cab based on coupled transfer path analysis. Automotive Innovation, 2(1), 26-34.

[23] Jiang, F., Ding, K., He, G., Sun, Y., & Wang, L. (2021). Vibration fault features of planetary gear train with cracks under time-varying flexible transfer functions. Mechanism and Machine Theory, 158, 104237.

[24] Meggitt, J. W. R., Elliott, A. S., Moorhouse, A. T., Jalibert, A., & Franks, G. (2021). Component replacement TPA: A transmissibility-based structural modification method for in-situ transfer path analysis. Journal of Sound and Vibration, 499, 115991.

[25] Almirón, J. O., Bianciardi, F., Corbeels, P., Pieroni, N., Kindt, P., & Desmet, W. (2022). Vehicle road noise prediction using component-based transfer path analysis from tire test-rig measurements on a rolling tire. Journal of sound and vibration, 523, 116694.

[26] Gajdatsy, P., Janssens, K., Desmet, W., & Van Der Auweraer, H. (2010). Application of the transmissibility concept in transfer path analysis. Mechanical Systems and Signal Processing, 24(7), 1963-1976.

[27] De Sitter, G., Devriendt, C., Guillaume, P., & Pruyt, E. (2010). Operational transfer path analysis. Mechanical Systems and Signal Processing, 24(2), 416-431.

[28] De Klerk, D., & Ossipov, A. (2010). Operational transfer path analysis: Theory, guidelines and tire noise application. Mechanical systems and signal processing, 24(7), 1950-1962.

[29] Van der Auweraer, H., Mas, P., Dom, S., Vecchio, A., Janssens, K., & Van de Ponseele, P. (2007). Transfer path analysis in the critical path of vehicle refinement: the role of fast, hybrid and operational path analysis.

[30] Shang, Z., Hu, F., Zeng, F., Wei, L., Xu, Q., & Wang, J. (2021). Research of transfer path analysis based on contribution factor of sound quality. Applied Acoustics, 173, 107693.

[31] Guo, R., Qiu, S., Fang, H. Q., Yu, Q. L., & Zhang, T. (2013). Advance in studying on transfer path analysis methods in frequency domain. Journal of Vibration and Shock, 32(13), 49-55.

[32] Gajdatsy, P., Janssens, K., Desmet, W., & Van Der Auweraer, H. (2010). Application of the transmissibility concept in transfer path analysis. Mechanical Systems and Signal Processing, 24(7), 1963-1976.

[33] Janssens, K., Gajdatsy, P., Gielen, L., Mas, P., Britte, L., Desmet, W., & Van der Auweraer, H. (2011). OPAX: A new transfer path analysis method based on parametric load models. Mechanical Systems and Signal Processing, 25(4), 1321-1338.

[34] Chu, Z., Xiong, M., Yang, Y., & He, Y. S. (2015). Time-domain transfer path analysis of automobile interior noise. J. Vib. Shock, 34(17), 161-166.

[35] Kong, L., Zhao, X., Yuan, X., Yu, Q., Zhou, C., Yang, Y., & Li, M. (2025). A novel operational transfer path analysis based on the complex-valued crosstalk elimination method. Measurement, 117813.